Dehydration of the molybdenum trioxide hydrates $MoO_3 \cdot nH_2O$: *in situ* x-ray absorption spectroscopy study at the Mo K edge

2000 J. Phys.: Condens. Matter 12 1959

(http://iopscience.iop.org/0953-8984/12/9/301)

J. Phys.: Condens. Matter **12** (2000) 1959–1970. Printed in the UK PII: S0953-8984(00)07059-4

Dehydration of the molybdenum trioxide hydrates $MoO_3 \cdot nH_2O$: *in situ* x-ray absorption spectroscopy study at the Mo K edge

Alexei Kuzmin and Juris Purans

Institute of Solid State Physics, University of Latvia, LV-1063 Riga, Latvia

Received 18 August 1999, in final form 29 November 1999

Abstract. The process of dehydration for the molybdenum trioxide hydrates, $MoO_3 \cdot 2H_2O \rightarrow \beta\text{-}MoO_3 \cdot H_2O \rightarrow \alpha\text{-}MoO_3$, was studied for the first time by *in situ* Mo K-edge x-ray absorption spectroscopy. A regularization procedure was applied to reconstruct the radial distribution functions around the molybdenum at all stages of the process. Strong variations in the local environment of the molybdenum were found at both phase transitions and were attributed to the changes in direction of the off-centre Mo displacement and in the degree of symmetrization of the Mo–O bonds. Also, an increase of the Mo–O–Mo angle, leading to the appearance of strong multiple-scattering effects in the x-ray absorption fine structure, was observed at the second phase transition $\beta\text{-}MoO_3 \cdot H_2O \rightarrow \alpha\text{-}MoO_3$. The final $\alpha\text{-}MoO_3$ product had nanocrystalline structure with an average grain size of about 15 Å.

1. Introduction

The crystallographic structure of the molybdenum trioxide hydrates or 'molybdic acids' $MoO_3 \cdot nH_2O$ ($n = 1, 2$) and $\alpha\text{-}MoO_3$ is related to that of a class of layer-type compounds (figure 1). Two-dimensional (2D) perovskite-like layers of distorted MoO_6 octahedra joined

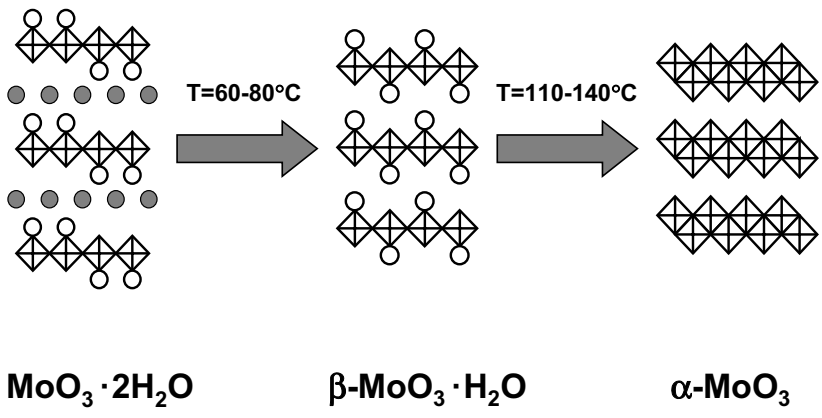

Figure 1. A schematic view of the crystalline structures of $MoO_3 \cdot 2H_2O$, $\beta\text{-}MoO_3 \cdot H_2O$, and $\alpha\text{-}MoO_3$ [1–5]. Open circles denote coordinated water molecules, whereas solid circles denote crystal water molecules. The temperature ranges for the two dehydration processes are also presented.

0953-8984/00/091959+12$30.00

by vertices exist in hydrates [1–3], whereas the 2D layers in α-MoO_3 are built up of double chains of edge-sharing MoO_6 octahedra connected through vertices [4, 5]. In both structures, the layers are stacked above each other with the voids in between. These voids are filled by crystal water molecules in molybdenum dihydrate $MoO_3{\cdot}2H_2O$ and are empty in monohydrate β-$MoO_3{\cdot}H_2O$ and α-MoO_3.

The six oxygen atoms of the distorted MoO_6 octahedron can be divided into two groups: bridging and terminal (or non-bridging). In all three compounds, one oxygen atom, pointing in the direction of the opposite layer, is terminal and strongly bound with a very short Mo–O distance, $\sim$1.69 Å [3–5]. The four oxygen atoms are bridging and form a skeleton of the layer: they have intermediate Mo–O distances ranging from 1.73 to 2.25 Å [3–5]. The sixth oxygen atom is located opposite to the first one at an Mo–O distance of 2.29–2.34 Å [3–5]. It corresponds to a terminal weakly bound water molecule in hydrates, while it is a bridging atom for the other two MoO_6 octahedra in α-MoO_3.

The process of dehydration for molybdenum trioxide hydrates has been studied in the past by means of x-ray diffraction (XRD) [1]; the results suggest a topotactic nature of the process $MoO_3{\cdot}2H_2O \rightarrow \beta$-$MoO_3{\cdot}H_2O \rightarrow \alpha$-$MoO_3$. Recently, a neutron powder thermo-diffractometric study [2] has been used to determine *in situ* long-range structural and kinetics information. The topotactic character has been confirmed; however, a slightly different model was proposed for the structure of the intermediate product β-$MoO_3{\cdot}H_2O$ [2]. The two studies [1] and [2] were concerned mainly with the long-range-order modifications occurring in the dehydration process, and, thus, the difference between the two models was related to the relative positioning of the opposite layers. In fact, it was suggested in [1] that dehydration results in the loss of the interlayer water molecules followed by a shrinkage of the MoO_6 octahedra sheets, whereas an additional relative displacement of each second MoO_6 layer in the perpendicular direction was found in [2]. That there is a similarity between the atomic arrangements of β-$MoO_3{\cdot}H_2O$ and $WO_3{\cdot}H_2O$ [6] was also stated in [2].

In the present work, the application of x-ray absorption spectroscopy allowed us to follow variations of the MoO_6 octahedra distortions during the dehydration process. The radial distribution functions (RDFs), reconstructed from the x-ray absorption fine structure (XAFS) by a regularization technique [7], show strong modifications of the local environment around molybdenum ions occurring at both stages of the process.

2. Experimental procedure

Polycrystalline yellow powder of monoclinic $MoO_3{\cdot}2H_2O$ was prepared as described in [2], and its single-phase structure was confirmed by x-ray powder diffraction. Experimental x-ray absorption spectra were recorded at the Mo K edge in the transmission mode at the LURE DCI storage ring on the D13 (EXAFS-3) beamline located at the bending magnet. The storage ring DCI operated at the energy 1.85 GeV and a maximum stored current of 315 mA. A standard transmission scheme with a Si(311) double-crystal monochromator and two ion chambers containing argon gas was used. The energy resolution was about 3 eV. The starting material, molybdenum dihydrate $MoO_3{\cdot}2H_2O$, was finely ground and mechanically mixed with boron nitride powder. The mixture was placed in a closed boron nitride cell mounted in a furnace. The sample had a thickness x, giving the value of the absorption jump $\Delta\mu\, x \simeq 1.0$. The measurements were performed on heating from room temperature (RT) to 400 °C in an oxidizing atmosphere. The temperature was stabilized to within $\pm$2 degrees during each measurement. The collected data cover the range of the two phase transitions: $MoO_3{\cdot}2H_2O \rightarrow \beta$-$MoO_3{\cdot}H_2O$ at 60–80 °C and β-$MoO_3{\cdot}H_2O \rightarrow \alpha$-$MoO_3$ at 110–140 °C [1, 2].

3. Data analysis

The x-ray absorption spectra were treated using the EDA software package [7].

In figure 2, the normalized x-ray absorption near-edge structures (XANES) $\mu(E)$ are shown for several temperatures. The E_0-position, defining the zero photoelectron wavevector value ($k = 0$), was set at the point (shown by vertical dotted line) found by the alignment of the experimental and calculated XAFS signals for α-MoO_3 [8,9]. The E_0-value was fixed for all spectra at the same energy.

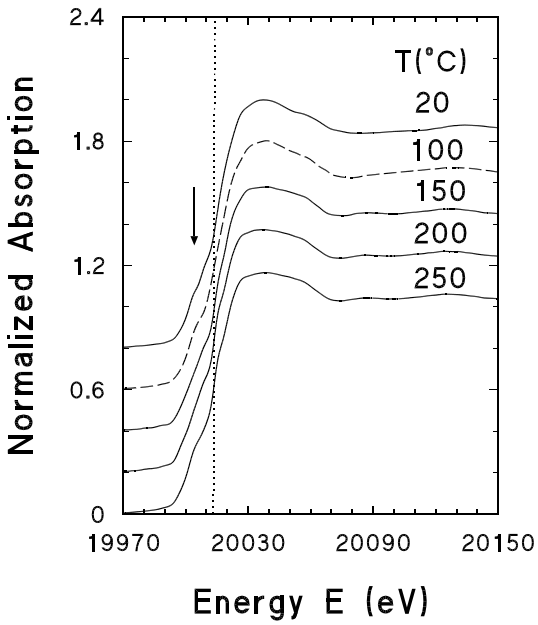

Figure 2. Variation of the normalized absorption coefficient $\mu(E)$ at the Mo K edge on dehydration of $MoO_3{\cdot}nH_2O$. The spectra are shifted along the vertical axis for clarity. The upper signal measured at $T = 20\ ^\circ$C corresponds to the starting yellow $MoO_3{\cdot}2H_2O$. The dashed line ($T = 100\ ^\circ$C) denotes the signal for yellow β-$MoO_3{\cdot}H_2O$. The lower three signals at $T \geqslant 150\ ^\circ$C correspond to white α-MoO_3. The arrow indicates the position of the pre-edge (the 1s(Mo) $\rightarrow$ 4d(Mo) + 2p(O) transition). The vertical dotted line shows the E_0-position used in the definition of the photoelectron kinetic energy.

The extracted experimental XAFS signals $\chi(k)k^2$ and their Fourier transforms (FTs) are shown in figure 3. The FTs were calculated in the range from 1.0 to 15.5 Å^{-1} with a Kaiser–Bessel window having the parameter $A = 2$ [7]. Note that since no phase correction was used in the FT calculations, the positions of the peaks in figure 3(b) differ from their true crystallographic values. The XAFS signals for the first coordination shell of molybdenum (see the dashed curves in figure 4) were calculated by the back-FT procedure within the range 0.2–2.2 Å, indicated in figure 3(b).

As one can see in figure 3(b), the first shell around the molybdenum is very broad and distorted, especially in the α-MoO_3 phase ($T \geqslant 150\ ^\circ$C) where two maxima are clearly visible in the FTs at $\sim$1 and $\sim$1.6 Å. This fact reflects the presence of different types of molybdenum–oxygen bonding in these structures with significantly varying Mo–O bond strengths [10]. Our experience [7] shows that the traditional methods of first-shell analysis, based on the multi-shell fitting procedure [11] or the single-shell cumulant approach [12], are not very suitable in

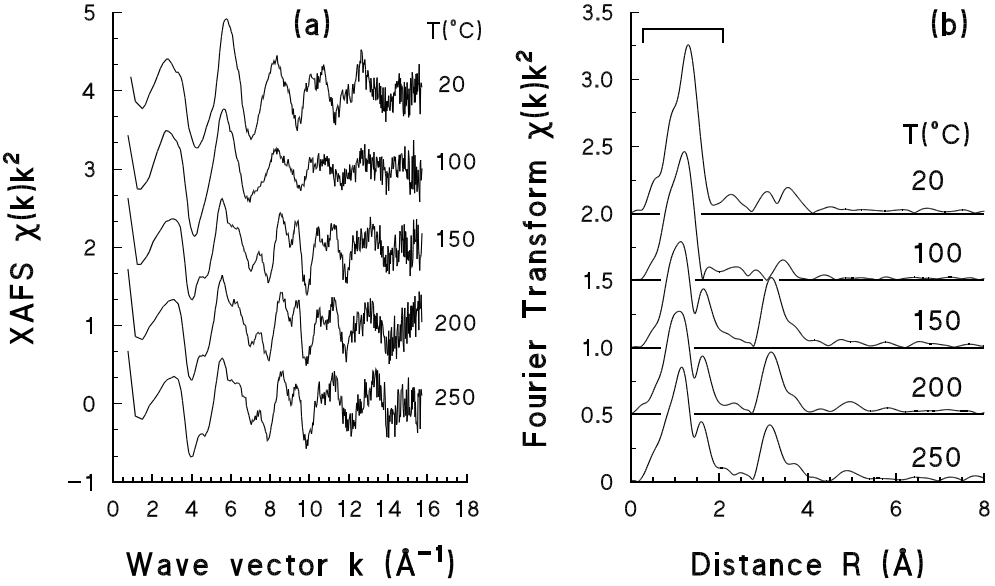

Figure 3. Experimental Mo K-edge XAFS $\chi(k)k^2$ signals (a) and their Fourier transforms (only moduli are shown) (b) corresponding to different steps of the $MoO_3{\cdot}nH_2O$ dehydration process. The range of the first coordination shell is indicated in (b). Note the strong change in the signals at the second dehydration step β-$MoO_3{\cdot}H_2O$ ($T = 100\ ^\circ$C) $\rightarrow$ α-MoO_3 ($T = 150\ ^\circ$C).

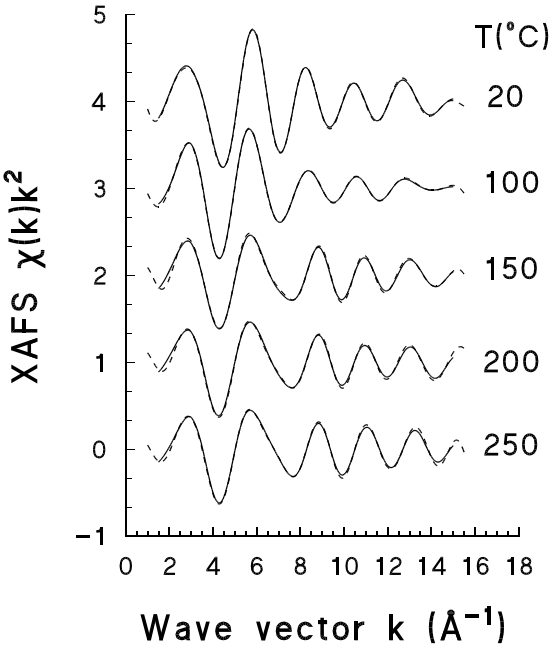

Figure 4. Calculated (solid curves) and experimental (dashed curves) XAFS $\chi(k)k^2$ signals for the first coordination shells around the molybdenum ions.

the case of such strong distortion, since the first method requires an *ad hoc* starting model and is not stable numerically, whereas the second method does not converge at all.

To overcome these difficulties and to obtain reliable and complete information from the analysis of the first-shell XAFS signals, we applied a method suggested by one of us

previously [7, 13, 14]. It is based on the regularization approach used to solve the standard least-squares problem:

$$S = \sum_{i=1}^{n} (\chi_{\text{exp}}(k_i) - \chi_{\text{model}}(k_i, G(R)))^2 \tag{1}$$

where $\chi_{\text{exp}}(k)$ is a set of experimental data and $\chi_{\text{model}}(k, G(R))$ is a model function defined by the general XAFS expression [15]

$$\chi_{\text{model}}(k, G(R)) = S_0^2 \int_{R_{\text{min}}}^{R_{\text{max}}} \frac{G(R)}{kR^2} F(\pi, k, R) \sin(2kR + \phi(\pi, k, R))\, \mathrm{d}R \tag{2}$$

with an arbitrary RDF $G(R)$, given on a mesh with the step $\mathrm{d}R$ in the range (R_{min}; R_{max}) of the first coordination shell. In equation (2), $k = \sqrt{(2m_e/\hbar^2)(E - E_0)}$ is the photoelectron wavevector; S_0^2 is the scale factor taking into account amplitude damping due to the multi-electron effects; R is the interatomic distance; $F(\pi, k, R)$ is the backscattering amplitude of the photoelectron, also accounting for its mean free path; $\phi(\pi, k, R) = \psi(\pi, k, R) + 2\delta_l(k) - l\pi$ is the phase shift containing contributions from the absorber $2\delta_l(k)$ and the backscatterer $\psi(\pi, k, R)$ (l is the angular momentum of the photoelectron, $l = 1$ for the K edge).

The RDF $G(R)$ is determined using the fast iteration procedure which requires only the calculation of the XAFS function $\chi_{\text{model}}(k, G(R))$ and its first derivative:

$$G(R_j) = G^0(R_j) + \left[\sum_{i=1}^{n} (\chi_{\text{exp}}(k_i) - \chi_{\text{model}}(k_i, G(R))) \frac{\partial \chi_{\text{model}}(k_i, G(R))}{\partial G(R_j)} \right] \times \left[\sum_{i=1}^{n} \left(\frac{\partial \chi_{\text{model}}(k_i, G(R))}{\partial G(R_j)} \right)^2 \right]^{-1} \tag{3}$$

where $G^0(R_j)$ denotes the value of $G(R_j)$ at the previous iteration. Two regularizing criteria are applied after each iteration to limit the shape of the RDF to physically significant solutions. First, $G(R)$ must be a non-negative function, so all negative values, when they exist, are changed to zeros. Second, the shape of $G(R)$ is expected to be a smooth function; therefore we apply a standard non-linear seven-point smoothing algorithm based on the third-order polynomial function to eliminate possible non-physical behaviour such as breaks, steps, and sharp needle-like peaks. One should remark that in the case of the Fourier filtered first-shell XAFS signal which we consider in the present work, the latter criterion was found to produce a small effect; however, it could be important for the case of virgin experimental data with a high noise contribution.

The starting approximation for $G(R)$ is chosen in an arbitrary manner on the mesh from R_{min} to R_{max} with a step $\mathrm{d}R$. In the present work, we tried different starting RDFs, set in the range of the first shell from $R_{\text{min}} = 0.8$ Å to $R_{\text{max}} = 2.6$ Å with the step $\mathrm{d}R = 0.02$ Å: they all resulted in the same final solution, which reflects the good convergence of the procedure. Note that the value of $\mathrm{d}R$ is related to the spatial resolution δR. Generally, when $\chi(k)$ is given in k-space from 0 to k_{max} with a step $\mathrm{d}k$, $G(R)$ is defined in R-space from 0 to $R_{\text{max}} \simeq \pi/(2\,\mathrm{d}k)$ with the spatial resolution $\delta R = 1/2k_{\text{max}}$ (e.g. $\delta R \simeq 0.03$ Å for $k_{\text{max}} = 16$ Å^{-1}) [16, 17]. The value of δR gives an estimate for the step $\mathrm{d}R$ used in (2): the latter should be smaller than the spatial resolution δR—otherwise the information contained in $\chi(k)$ can be lost—but, at the same time, it should be large enough to allow the convergence and stability of the fitting procedure. Note that the use of a smaller value of $\mathrm{d}R$ than is given by δR is also possible due to the smoothness criterion which imposes an additional constraint on the shape of the RDF $G(R)$. Our experience shows that a value of $\mathrm{d}R = 0.01$–0.02 Å can be used in most cases.

The method described was successfully tested on several model compounds and showed a wider range of applicability than traditional approaches [7]. Its previous use for the reconstruction of the first-shell RDFs of crystalline and disordered materials can be found in references [7, 13, 14, 18].

The backscattering amplitudes and phase shifts, used in equation (2), were calculated using the FEFF6 code [19]. The calculations were performed for two clusters with the radius 8 Å having the crystal structures of $MoO_3{\cdot}2H_2O$ [3] and α-MoO_3 [4, 5] and centred at the molybdenum atom. The muffin-tin radii were chosen according to the Norman criterion [20] and were reduced by a factor of 0.8. They were equal to 1.073 Å for the absorber (Mo) and 0.800 Å (O) and 1.068 Å (Mo) for the neighbouring atoms. The complex Hedin–Lundqvist potential [22] was used to describe the exchange and correlation effects; therefore $F(\pi, k, R)$ automatically included the correction to the mean free path. Natural broadening was included through the core-level width $\Gamma_{\text{core hole}}(\text{K–Mo}) = 5.7$ eV [21]. The calculated scattering amplitude and phase-shift functions for the nearest oxygen atoms, located in the first shell at different distances from the central molybdenum atom, were compared to estimate the significance of the photoelectron wave curvature effect on $F(\pi, k, R)$ and $\phi(\pi, k, R)$. It was found that the effect is negligible within the first shell; therefore, the functions $F(\pi, k, R_{\text{const}})$ and $\phi(\pi, k, R_{\text{const}})$ calculated for the mean Mo–O distance $R_{\text{const}} = 1.9$ Å were used in the regularization procedure. The value of S_0^2 was fixed at 0.8 on the basis of the best fit of the α-MoO_3 XAFS signal.

As a result of the regularization process, the RDF $G(R)$ and corresponding XAFS $\chi(k)k^2$ were obtained for each experimental first-shell signal. A comparison of calculated and experimental XAFS signals, shown in figure 4 by solid and dashed lines, respectively, indicates a very good agreement between them, and, therefore, suggests high reliability of the RDFs $G(R)$ presented in figure 5. Note that the first-shell RDFs for each of the phases are significantly

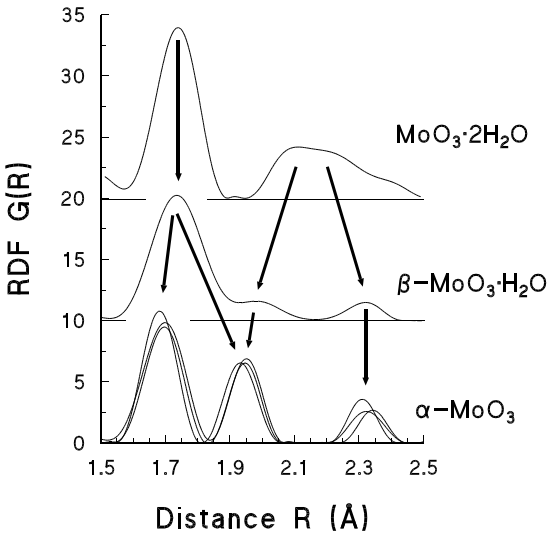

Figure 5. The radial distribution functions (RDFs) $G(R)$ around molybdenum ions within the first-coordination-shell range: upper curve: $T = 20$ °C (yellow $MoO_3{\cdot}2H_2O$); middle curve: $T = 100$ °C (yellow β-$MoO_3{\cdot}H_2O$); and lower curves: $T = 150$, 200, and 250 °C (white α-MoO_3). The RDFs correspond to the calculated XAFS signals shown in figure 4. The arrows indicate the process of the subshell splitting. Note that the RDFs vary strongly at both dehydration steps, especially in the region of distant oxygen ions ($R > 1.85$ Å).

different. Their accuracy can be estimated by comparison of the $G(R)$ functions for α-MoO_3, obtained for several temperatures (see the lower three curves in figure 5). They should differ due to the temperature effect, which results in additional broadening of peaks for higher temperature. The observed differences are small enough, being much smaller than that between RDFs for the three phases. This fact and the good agreement between the XAFS signals (figure 4) suggest, at least, high relative accuracy of the RDFs $G(R)$.

To discuss the RDFs obtained quantitatively, we used Gaussian approximation as a model for $G(R)$. A set of structural parameters (see table 1) such as the coordination numbers (N), the Mo–O distances (R), and the mean square relative displacements (MSRDs) σ^2, related to the thermal and static disorder, were determined by the best-fit procedure with the model function, consisting of three Gaussian lines, applied to the RDFs in figure 5. Since one deals with crystalline materials, we only allowed the coordination numbers to take integer values in the fit. Note that N is determined by the area under the peak, R by the peak position, and 2σ by the width of the peak at half height.

Table 1. Structural parameters for $MoO_3{\cdot}nH_2O$ ($n = 0, 1, 2$) determined within the Gaussian approximation from the RDF reported in figure 5. N is the coordination number: it was restricted, from crystallographic considerations, to integer values, which gives the best agreement between the RDF obtained and its Gaussian model. R is the Mo–O distance (±0.01–0.05 Å), and σ^2 is the MSRD for the Mo–O bond (±0.002–0.005 Å^2). The average values for three temperatures are reported for α-MoO_3.

	$MoO_3{\cdot}2H_2O$ $T = 20\,^\circ$C			β-$MoO_3{\cdot}H_2O$ $T = 100\,^\circ$C			α-MoO_3 $T = 150$, 200, and 250 $^\circ$C		
N	3	1	1	3	1	1	2	2	1
R	1.74	2.10	2.26	1.74	1.98	2.32	1.69	1.95	2.31
σ^2	0.003	0.006	0.017	0.006	0.010	0.012	0.003	0.005	0.006

4. Results and discussion

4.1. XANES

The Mo K-edge x-ray absorption near-edge structure (XANES) spectra, for different stages of the dehydration process of $MoO_3{\cdot}2H_2O$, are shown in figure 2. The first spectrum, measured at 20 °C, corresponds to the starting $MoO_3{\cdot}2H_2O$ compound, which transforms at 60–80 °C [1,2] to monohydrate β-$MoO_3{\cdot}H_2O$ (dashed line, $T = 100\,^\circ$C). A second step of the reaction occurs at 110–140 °C [1, 2]; therefore the last three spectra at 150, 200, and 250 °C correspond to α-MoO_3. Note that the low resolution at the Mo K edge, which is due to the large natural broadening equal to ∼5.7 eV [21], results in a smearing of the details in the XANES region.

A typical characteristic of the Mo K-edge region in the series is the presence of a pre-edge shoulder (indicated by an arrow in figure 2), located below the continuum threshold E_0 (shown by the vertical dotted line). Its originates from the $1s(Mo) \rightarrow \overline{4, \epsilon}d(Mo) + \overline{2, \epsilon}p(O)$ transition, in which the final state of the electron is the relaxed excited state in the continuum (ϵ) with 4d(Mo) atomic character in the presence of the core hole at the 1s(Mo) level screened by other electrons. Since such a transition is forbidden in the dipole approximation for a perfect octahedron, the pre-edge shoulder amplitude depends on the degree of the MoO_6 octahedron distortion and of that of the 2p(O)–4d(Mo) hybridization. As will be shown below, the MoO_6 octahedra in all three compounds are strongly distorted, which explains the origin of the pre-edge shoulder. The similarity of the shoulders in all the spectra indicates that the nearest group

of oxygen atoms, located at 1.69–1.74 Å and present for both hydrates and trioxide, gives rise to the main contribution to producing it.

4.2. XAFS

The experimental XAFS $\chi(k)k^2$ signals, presented in figure 3(a), show complex oscillating structure over the whole k-space range. It is interesting that (1) their amplitude does not diminish when the temperature rises by more than 200 °C; moreover, (2) the signals at low temperatures are more structureless than those at high temperatures. The first fact indicates a strong bonding between absorbing molybdenum and neighbouring oxygen atoms, which produce the main contribution to the XAFS (note the small values of the MSRDs, σ^2(Mo–O) $\simeq$ 0.003–0.005 Å^2, for the nearest group of oxygens in table 1). The second fact suggests that a contribution from outer shells, which are responsible for the production of the high-frequency XAFS signals, increases at the phase transition β-$MoO_3{\cdot}H_2O \rightarrow \alpha$-$MoO_3$. This can be readily observed in figure 3(b) as an increase of the second-shell peak at ~3–3.5 Å. At the same time, one can observe no significant variation of the peak intensity at longer ($R > 4.5$ Å) distances.

First, we will discuss the transformations occurring on dehydration in the first coordination shell of molybdenum. The RDFs $G(R)$ in figure 5 show unambiguously that the dehydration process is accompanied by strong changes of the first-shell MoO_6 octahedron distortion. This result complements the findings of the previous works [1, 2], where the dehydration process was mainly related to the loss of crystal water molecules and topotactic rearrangements of the MoO_6 octahedra. As one can see in figure 5, the long Mo–O bonds ($R > 1.85$ Å) experience most transformations, whereas the group of short Mo–O bonds (the first peak at 1.7 Å) changes less extensively.

On the basis of the results of the Gaussian decomposition (table 1), we propose the following model for the variation of the MoO_6 octahedron distortion. In $MoO_3{\cdot}2H_2O$ at 20 °C, the molybdenum ions are displaced off-centre in the ⟨111⟩ direction leading to the distortion of the MoO_6 octahedra, which manifests itself as a splitting into two subshells (or groups) composed of three oxygen atoms each. The three oxygen atoms of the nearest subshell are located at the mean distance 1.74 ± 0.01 Å, which is in good agreement with that (1.75 Å) determined by means of XRD in [3]. The MSRD value $\sigma^2 = 0.004 \pm 0.002$ Å^2 is comparable with that determined from the static distribution of the Mo–O nearest bonds (from 1.680 to 1.822 Å [3]) and, thus, suggests a small thermal contribution and strong Mo–O bonding. The distribution of the long Mo–O bond lengths is very broad and can be well approximated by two contributions from oxygen atoms located at 2.10 ± 0.03 Å with $\sigma^2 = 0.006 \pm 0.003$ Å^2 and at 2.26 ± 0.05 Å with $\sigma^2 = 0.017 \pm 0.005$ Å^2. The mean value for the peak position is 2.17 ± 0.05 Å and for σ^2 is 0.015 ± 0.005 Å^2, which can be compared with the XRD data [3]: 2.17 Å and a distribution ranging from 2.041 to 2.301 Å.

One should point out that the coordination number determined for the group of oxygen atoms with the longest bonds is smaller by one atom in our analysis (table 1) compared to that in [3]. This also happens for the other two phases, β-$MoO_3{\cdot}H_2O$ and α-MoO_3. We attribute this discrepancy to the fact that the contributions of the coordinated water molecule in hydrate [3, 5] and of the most distant oxygen atom at 2.34 Å in trioxide [4] to the XAFS signals are very weak and difficult to detect. Such an explanation is supported by the formal bonding conditions. Molybdenum ions have the formal valence state of 6+ and, thus, donate six electrons to oxygen ions. Since the terminal oxygen atom is formally bound by a double bond which involves two electrons from molybdenum, the molybdenum atom can additionally make bonds with four bridging oxygens, each being shared between two molybdenum atoms.

Thus, the molybdenum atoms are formally bound to five oxygens observed by means of XAFS. The sixth oxygen atom belongs to a coordinated water molecule in hydrates or is an atom that is bridging for another two molybdenum atoms in trioxide. It formally completes the MoO_6 octahedron, but is weakly bound [5] and, therefore, its contribution to the XAFS may be strongly damped.

At 60–80 °C, dihydrate $MoO_3{\cdot}2H_2O$ loses interlayer water molecules and transforms into β-$MoO_3{\cdot}H_2O$ [1, 2]. In previous works [1, 2], this phase transition was mainly related to the topotactic changes of the structure, which were associated with a collapse of the two-dimensional perovskite-like layers along the *b*-axis. An additional cooperative shift between each pair of consecutive layers was proposed in [2]. However, in both [1] and [2] there is a lack of information on modifications occurring within MoO_6 octahedra. Our results in figure 5 show that the phase transition is also accompanied by changes in the MoO_6 octahedra distortion which mainly affects the group of distant oxygen atoms. The mean distance (1.74 ± 0.01 Å) and the number (3) of oxygen atoms in the nearest group remains unchanged, and only a slight increase of the MSRD value to $\sigma^2 = 0.005 \pm 0.001$ Å^2 occurs. However, the group of distant oxygen atoms becomes split, with the result that two oxygen atoms are now located at mean distances equal to 1.98 ± 0.02 Å and 2.32 ± 0.02 Å with the MSRDs $\sigma^2 = 0.014 \pm 0.005$ Å^2 and 0.02 ± 0.005 Å^2, respectively. The observed type of MoO_6 octahedra distortion suggests that, as in dihydrate, molybdenum atoms in monohydrate are displaced off-centre in the $\langle 111 \rangle$ direction. Also as for $MoO_3{\cdot}2H_2O$, the total number of oxygen atoms detected by means of XAFS in the first shell is five; the sixth atom of the water molecule was not found within the accuracy of the present data.

The phase transition from β-$MoO_3{\cdot}H_2O$ to α-MoO_3 occurs at 110–140 °C [1, 2]. It is accompanied by significant modifications of the layer structure: the perovskite-like 2D sheets of vertex-sharing MoO_6 octahedra in monohydrate lose coordinated water molecules and collapse topotactically into a bilayer structure built up of MoO_6 octahedra each sharing two edges [4]. A possible mechanism for the transformation was suggested in [2]. From the local point of view, the second step of the dehydration process is accompanied by dramatic changes of the RDF. In spite of the high temperature ($T \geqslant 150$ °C) at which the *in situ* measurements were performed, one observes three well defined peaks in the first coordination shell (figure 5). The first peak corresponds to two oxygen atoms at 1.69 ± 0.02 Å with the MSRD $\sigma^2 = 0.003 \pm 0.002$ Å^2, the second peak is due to two oxygen atoms at 1.95 ± 0.02 Å with the MSRD $\sigma^2 = 0.005 \pm 0.003$ Å^2, and the third peak corresponds to one oxygen atom at 2.31 ± 0.05 Å with the MSRD $\sigma^2 = 0.006 \pm 0.004$ Å^2. According to XRD results [4], the six oxygen atoms are located at the distances 1.68, 1.73, 1.95, 1.95, 2.25, and 2.34 Å from the central molybdenum atom. Again, the sixth oxygen atom of the MoO_6 octahedron was not detected by means of XAFS. Thus, as shown in figure 5 by arrows, during the transformation β-$MoO_3{\cdot}H_2O \rightarrow \alpha$-$MoO_3$, one oxygen atom is split off the nearest group of oxygens at 1.74 Å and forms, together with the atom at 1.98 Å, a middle subshell at 1.95 Å. This type of distortion corresponds to the molybdenum atoms displaced off-centre in the $\langle 110 \rangle$ direction. It is interesting that in spite of the temperature increase, the MSRD values for each oxygen subshell become smaller in trioxide than in monohydrate and also dihydrate. This suggests stronger Mo–O bonding and that the structure of trioxide is more rigid/stable than that of hydrates.

A feature common to the three compounds is the presence of a ferroelectric distortion [5, 23] along one (in α-MoO_3) and two (in $MoO_3{\cdot}2H_2O$ and β-$MoO_3{\cdot}2H_2O$) molybdenum–oxygen–molybdenum chain(s). This distortion is responsible for the off-centre molybdenum displacement and gives rise to alternating short and long Mo–O bonds [5]. A comparison of the RDFs in figure 5 suggests that the presence of the interlayer water molecules in dihydrate

partially stabilizes the ferroelectric distortion along one (1.80 and 2.05 Å) of the chains, which tends towards symmetrization (∼1.87 and 1.98 Å) in monohydrate and becomes symmetric (1.95 and 1.95 Å) in trioxide. This means that the interlayer water influences the charge redistribution within the molybdenum–oxygen layers.

Finally, we would like to discuss the variations occurring on dehydration of $MoO_3 \cdot 2H_2O$ within the outer shells (peaks at $R > 2.8$ Å in figure 3(b)), composed of molybdenum atoms.

It is well known [24–27] that the XAFS from octahedrally coordinated systems, especially with linear or near-linear atomic chains, is strongly affected by the presence of multiple-scattering (MS) signals, which contribute in FTs beyond the first shell. The presence of the MS signals significantly complicates the analysis of the outer shells, especially for low-symmetry compounds where a lot of non-equivalent scattering paths should be taken into account. However, the strong sensitivity of the MS signal amplitude to the values of the bonding angles in atomic chains that are close to linear opens up new possibilities for at least qualitative analysis. From XRD data [3], the vertex-sharing MoO_6 octahedra in $MoO_3 \cdot 2H_2O$ have the values of the Mo–O–Mo angles in the range from 140.6 to 161.5 degrees with the mean value ∼150 degrees. It is known [28, 29] that this value is small enough to give rise to strong MS contributions; therefore the amplitude of the second-shell peak at 3–3.5 Å in the FT (figure 3(b)) is not high. The second-shell amplitude remains nearly the same in β-$MoO_3 \cdot H_2O$, suggesting the absence of near-linear Mo–O–Mo chains in the structure of monohydrate. Upon transition to α-MoO_3, the second-shell peak increases instantaneously (figure 3(b)) due to an increase of the Mo–O–Mo angle value along one of the crystallographic axes [4]. The MS effects within this chain are responsible for the strong high-frequency signal visible in the XAFS in figure 3(a) and for the increase of the second-shell peak at 3 Å in figure 3(b) [8]. It is important to point out that in the present case, the amplification of the XAFS due to the MS contribution overwhelms the thermal damping, so the second-shell XAFS in α-MoO_3 changes slightly in the range from 150 to 250 °C.

Finally, we would like to estimate the size of the crystallites produced during the dehydration process. In figure 6, we compare the FT of the XAFS signal for α-MoO_3 (solid line), which is the dehydration product of $MoO_3 \cdot 2H_2O$, with that for the commercial polycrystalline α-MoO_3 powder (dashed line). The two signals are only different in amplitude, so we present only the moduli of the FTs. The two XAFS spectra were measured at the same temperature, $T = 200$ °C; therefore a similar influence of the thermal disorder on the XAFS (and thus the FT) amplitude is expected. However, a strong difference in the amplitude of the outer-shell peaks (indicated by arrows in figure 6) is observed, and this can be attributed to a difference in crystallite size.

The authors in [2] determined from the broadening of the Bragg peaks in neutron diffraction patterns that the grain sizes of α-MoO_3 obtained during dehydration are around 50–150 Å at 200 °C. These values are much smaller than that for our commercial polycrystalline α-MoO_3 powder, which has grain sizes of a few microns. From the studies of nanocrystalline nickel oxide [30], we know that such a difference in size of the crystallites may be responsible for the XAFS amplitude damping being similar to that observed in figure 6. Following the approach described in [30], the average grain size in our experiment was estimated, on the basis of the reconstructed grain-boundary model [31], from the amplitude ratios of the FT peaks related to the molybdenum-containing shells. The ratios obtained are 0.75, 0.59, and 0.43, respectively, for the three peaks at 3.2, 5.0, and 5.8 Å (figure 6). The final estimate of the average grain size for α-MoO_3 at 200 °C is equal to ∼15 Å. This value is smaller than that from the neutron diffraction study [2], but it could be underestimated because the model used [30] assumes close-packed spherical grains, which is not appropriate for layer-type α-MoO_3 structure [4].

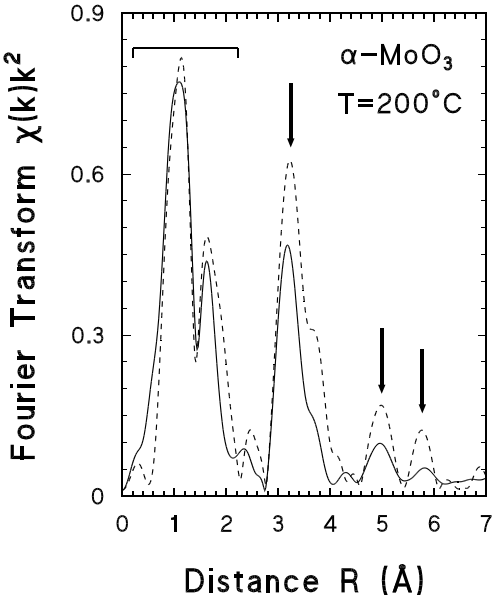

Figure 6. The FT modulus of the XAFS signals $\chi(k)k^2$ for α-MoO_3 at 200 °C. The solid line corresponds to α-MoO_3 obtained on dehydration of $MoO_3{\cdot}2H_2O$; the dashed line corresponds to commercial polycrystalline α-MoO_3 powder. The range of the first coordination shell ($R < 2.2$ Å) is shown by the bracket. The arrows indicate the positions of the peaks, which correspond to outer shells composed mainly of molybdenum atoms; strong decrease of the peak amplitude is clearly visible and is attributed to a difference in crystallite size.

5. Summary and conclusions

We present for the first time an *in situ* Mo K-edge x-ray absorption spectroscopy study of the dehydration process $MoO_3{\cdot}2H_2O \rightarrow \beta$-$MoO_3{\cdot}H_2O \rightarrow \alpha$-$MoO_3$. Using a regularization procedure, we reconstructed the radial distribution functions (RDFs) around molybdenum at the all stages of the process and, thus, determined precisely the modifications of the MoO_6 octahedra distortion. The results obtained were compared with those determined by diffraction techniques in [1, 2].

In spite of some similarity of the structural models proposed in [1, 2] on the basis of diffraction data for two hydrates, we found that the first-shell RDF is different for dihydrate and monohydrate. Strong variations in the local environment of molybdenum at the two phase transitions were observed and attributed to the changes in direction of the off-centre Mo displacement and in the degree of symmetrization of the Mo–O bonds. Quantitative analysis of the second-shell signals allowed us to conclude that, as opposed to the case for α-MoO_3, the values of all Mo–O–Mo angles in hydrates are far from 180°.

The crystallinity of the final product α-MoO_3 was estimated from the degree of reduction of the outer-shell amplitude. The calculations using the reconstructed grain-boundary model [30, 31] suggested an average grain size of about 15 Å.

Acknowledgments

JP is indebted to the LURE laboratory for providing the beam time and partial support. He is grateful to Professor S Benazeth and Dr Ph Parent for assistance during XAS experiments.

This work was supported in part by the Latvian Government Research Grants No 93.652 and No 96.0670.

References

[1] Günter J R 1972 *J. Solid State Chem.* **5** 354
[2] Boudjada N, Rodriguez-Carvajal J, Anne M and Figlarz M 1993 *J. Solid State Chem.* **105** 211
[3] Krebs B 1972 *Acta Crystallogr.* B **28** 2222
[4] Kihlborg L 1963 *Ark. Kemi* **21** 357
[5] Crouch-Baker S and Dickens P G 1989 *Solid State Ion.* **32+33** 219
[6] Szymanski J T and Roberts A C 1984 *Can. Mineral.* **22** 681
[7] Kuzmin A 1997 *J. Physique Coll.* IV **7** C2 213
Kuzmin A 1995 *Physica* B **208+209** 175
Kuzmin A 1996 *EDA: EXAFS Data Analysis Software Package. User's Manual* (available from the author at http://www.dragon.lv/eda)
[8] Kuzmin A and Purans J 1993 *J. Phys.: Condens. Matter* **5** 267
[9] Purans J, Kuzmin A, Parent Ph and Dexpert H 1995 *Physica* B **208+209** 307
[10] Nazri G A and Julien C 1992 *Solid State Ion.* **53–56** 376
[11] Crozier E D, Rehr J J and Ingals R 1988 *X-Ray Absorption: Principles, Applications, Techniques of EXAFS, SEXAFS and XANES* ed D C Koningsberger and R Prins (New York: Wiley) p 373
[12] Bunker G 1983 *Nucl. Instrum. Methods* A **207** 437
[13] Kuzmin A, Purans J, Dalba G, Fornasini P and Rocca F 1996 *J. Phys.: Condens. Matter* **8** 9083
[14] Kuzmin A and Purans J 1997 *Proc. SPIE* **2968** 180
Kuzmin A and Purans J 1997 *J. Physique Coll.* IV **7** C2 971
Kuzmin A, Purans J, Parent Ph and Dexpert H 1997 *J. Physique Coll.* IV **7** C2 891
[15] Stern E A and Heald S M 1983 *Handbook of Synchrotron Radiation* ed E E Koch (New York: North-Holland) ch 10
[16] Lanczos C 1956 *Applied Analysis* (Englewood Cliffs, NJ: Prentice-Hall)
[17] Stern E A, Ma Y, Hanske-Petitpierre O and Bouldin C E 1992 *Phys. Rev.* B **46** 687
[18] Rocca F, Dalba G, Grisenti R, Bettinelli M, Monti F and Kuzmin A 1998 *J. Non-Cryst. Solids* **232–234** 581
Rocca F, Dalmasso A, Monti F, Kuzmin A and Pasqualini D 1999 *J. Synchrotron Radiat.* **6** 737
[19] Rehr J J, Zabinsky S I and Albers R C 1992 *Phys. Rev. Lett.* **69** 3397
Rehr J J, Mustre de Leon J, Zabinsky S I and Albers R C 1991 *J. Am. Chem. Soc.* **113** 5135
Mustre de Leon J, Rehr J J, Zabinsky S I and Albers R C 1991 *Phys. Rev.* B **44** 4146
[20] Norman J G 1974 *Mol. Phys.* **81** 1191
[21] Keski-Rahkonen O and Krause M O 1974 *At. Data Nucl. Data Tables* **14** 139
[22] Hedin L and Lundqvist B I 1971 *J. Phys. C: Solid State Phys.* **4** 2064
[23] Goodenough J B 1967 *Mater. Res. Bull.* **2** 165
[24] Alberding N, Crozier E D, Ingals R and Houser B 1986 *J. Physique* **47** 681
[25] Vedrinskii R V, Bugaev L A and Levin I G 1988 *Phys. Status Solidi* b **150** 307
[26] Mustre de Leon J, Yacoby Y, Stern E A, Rehr J J and Dell'Ariccia M 1989 *Physica* B **158** 263
[27] Kuzmin A, Purans J, Benfatto M and Natoli C R 1993 *Phys. Rev.* B **47** 2480
[28] Kuzmin A and Purans J 1993 *J. Phys.: Condens. Matter* **5** 9423
[29] Kuzmin A, Purans J and Parent Ph 1995 *Physica* B **208+209** 45
[30] Kuzmin A, Purans J and Rodionov A 1997 *J. Phys.: Condens. Matter* **9** 6979
[31] Löffler J and Weissmüller J 1995 *Phys. Rev.* B **52** 7076